Controlled Load and Speed Transitions in a Multicylinder Recompression HCCI Engine

Shyam Jade, *Student Member, IEEE*, Jacob Larimore, *Student Member, IEEE*, Erik Hellström, *Member, IEEE*, Anna G. Stefanopoulou, *Fellow, IEEE*, and Li Jiang

***Abstract*— A model-based control strategy to track combustion phasing during load and speed transitions in the homogeneous charge compression ignition (HCCI) operating region of a multimode combustion engine is presented in this paper. HCCI transitions can traverse regions of high cyclic variability (CV), even if the steady state transition end points are stable with low CV. A control-oriented HCCI model for both the stable, low CV region and the oscillatory, high CV, late phasing region is used to design a controller that uses valve and fuel injection timings to track combustion phasing. Novel aspects of the controller include nonlinear model-inversion-based feedforward and gain scheduled feedback based on unburned fuel that reduces transient CV. Transitions tested on a multicylinder HCCI engine include load transitions at fixed engine speeds, simultaneous load, and speed transitions, and select FTP75 drive-cycle transitions with high load slew rates. Good combustion phasing tracking performance is demonstrated, and misfires are prevented.**

***Index Terms*— Advanced combustion, cyclic variability (CV), homogeneous charge compression ignition (HCCI) combustion, internal combustion engines, nonlinear dynamical systems.**

I. Introduction

HOMOGENEOUS charge compression ignition (HCCI) combustion is a low-temperature combustion strategy characterized by near simultaneous compression-driven autoignition events at multiple sites throughout a uniformly mixed air–fuel mixture [1], [2]. Although high thermal efficiency and low engine out emissions make this combustion mode attractive, there are a number of outstanding control challenges that are yet to be solved. This paper aims to advance the state of art by proposing a transient controller to track combustion phasing during load–speed transitions in the HCCI operating space.

Fig. 1 shows the load–speed operating map of the multimode combustion engine. Some sample HCCI transitions from an FTP75 drive-cycle simulation [3] involving simultaneous variations in both load and speed are demonstrated. To maximize the length of stay in the HCCI region, and hence the efficiency benefit, it is important to demonstrate quick and stable control of these transitions. This is a key practical component in the effort to expand the HCCI operating space.

Autoignition timing control in HCCI combustion is relatively insensitive to spark timing, and requires careful regulation of the temperature, pressure, and composition of the precombustion charge. Further, the combustion phasing or location is constrained within a limited acceptable range by pressure rise rate and stability constraints [4], [5, Fig. 2]. Late phasing can lead to incomplete combustion, the retention

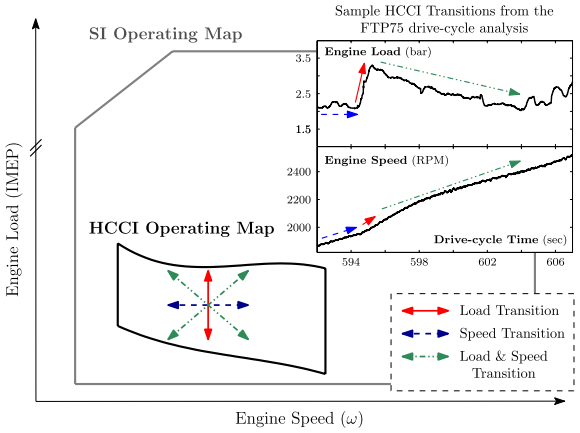

Fig. 1. Load–Speed operating map of the engine showing HCCI and SI regions with representative HCCI transitions from an FTP75 drive-cycle analysis [3].

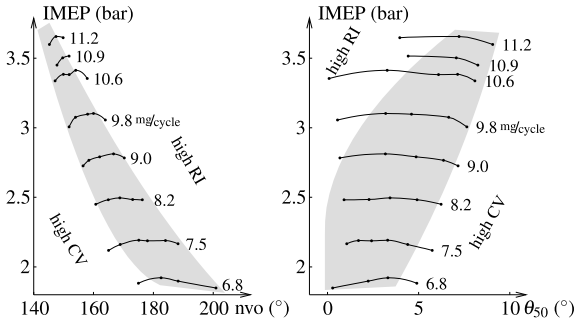

Fig. 2. Single cylinder engine experiments for the usable HCCI operating region at 2000 revolutions/min. The acceptable combustion phasing range, represented by θ_{50}, is limited by ringing intensity and CV constraints [5].

Manuscript received November 19, 2013; revised May 19, 2014; accepted July 28, 2014. Date of publication September 5, 2014; date of current version April 14, 2015. Manuscript received in final form August 5, 2014. This work was supported in part by the National Energy Technology Laboratory, Department of Energy, Morgantown, WV, USA, under Award DE-EE0003533 and in part by the ACCESS Project Consortium, including Robert Bosch LLC, Farmington Hills, MI, USA, AVL Inc., Plymouth, MI, USA, and Emitec Inc., Rochester Hills, MI, USA. Recommended by Associate Editor L. Del Re.

S. Jade, J. Larimore, E. Hellström, and A. G. Stefanopoulou are with the Department of Mechanical Engineering, University of Michigan, Ann Arbor, MI 48109 USA (e-mail: sjade@umich.edu; larimore@umich.edu; erik.hellstrom@gmail.com; annastef@umich.edu).

L. Jiang is with the Department of Gasoline System Engineering, Robert Bosch LLC, Farmington Hills, MI 48331 USA (e-mail: li.jiang@us.bosch.com).

Color versions of one or more of the figures in this paper are available online at http://ieeexplore.ieee.org.

Digital Object Identifier 10.1109/TCST.2014.2346992

of significant amounts of unburned fuel between cycles, and in extreme cases, engine misfire. Carefully constraining combustion phasing is of specific concern during transients, when the combustion can pass through a region of high cyclic variability (CV), even if the starting and ending steady-state points demonstrate stable, low CV behavior.

An HCCI combustion model is developed that combines prior work by the authors on the modeling of HCCI combustion dynamics both in the stable low CV region [6]–[10], and in the oscillatory high CV late phasing region [4], [11]–[17]. Validation results show that the model captures the steady-state behavior in both the dynamic regions and the onset of high CV. A model-based controller is designed that uses valve and fuel injection timings to track desired combustion phasing during HCCI load–speed transitions. Contributions in the controller design include the use of nonlinear model-inversion-based feedforward and gain scheduling feedback. The feedback block aims to detect if the combustion is in a high CV or a low CV region based on predicted unburned fuel mass, and applies a different control signal in each CV region.

The comprehensiveness of the experimental results is another important contribution. Some HCCI control strategies found in the literature are validated to track steps in desired combustion phasing at a single load–speed HCCI operating point [18], [19]. Others regulate combustion phasing during load steps at a fixed engine speed [20]–[23] or track steps in desired location and magnitude in peak pressure [24], [25]. In this paper, the same controller is shown to work well for a number of different transitions in the HCCI operating space, instead of for a single scenario. Transitions tested on the multicylinder HCCI engine include load transitions at fixed engine speeds, simultaneous load and speed transitions, and select FTP75 drive-cycle transitions with high load slew rates. Good combustion phasing tracking performance is demonstrated, and misfires are prevented.

The paper is organized as follows. Section II introduces the experimental HCCI setup used to implement and test the controllers. The control actuators and performance outputs of the system are described. A physical understanding of the onset of high CV dynamics in HCCI is discussed in Section III. The low-order control-oriented model is presented in Section IV, along with validation results. This model is used in Section V to design the combustion phasing tracking controller. In Section VI, experimental results demonstrating the successful control of various transitions are presented. These transitions involve a combination of engine load and speed variations. Finally, the conclusion and future work are discussed in Section VII.

II. Experimental Multicylinder HCCI Engine

Recompression, the strategy used in this paper, is an efficient and relatively quick actuation strategy for affecting the temperature of the precombustion charge in HCCI combustion [26]. In recompression HCCI, the exhaust valve is closed early and the intake valve is opened late, compared with typical spark ignition operation. The resulting negative valve overlap (NVO) can be observed in the typical recompression

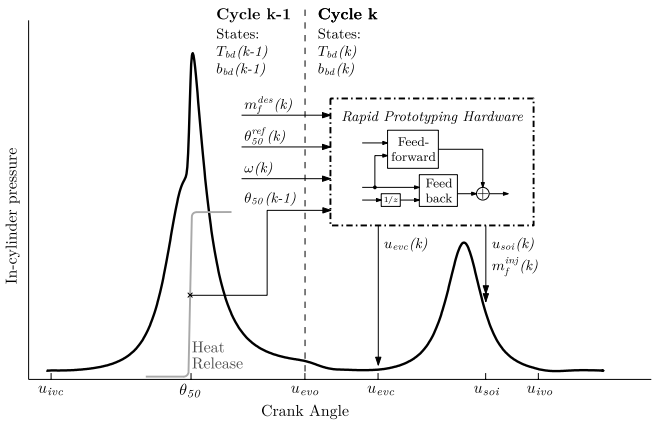

Fig. 3. Typical recompression HCCI pressure trace, showing the relative locations of inputs, outputs, and states. The feedback/feedforward controller implemented in the rapid prototyping hardware uses the feedback output θ_{50} to control u_{evc}, u_{soi}, and m_f^{inj} of the next cycle. HCCI transitions are externally specified as a combination of m_f^{des}, θ_{50}^{ref}, and ω.

HCCI in-cylinder pressure trace in Fig. 3 as the second pressure rise event. A large fraction of the in-cylinder charge is trapped before it can be exhausted. These hot residual gases that are retained between engine cycles have a significant impact on the temperature and composition of the in-cylinder charge of the subsequent cycle.

A turbocharged direct-injection inline four-cylinder GM LNF Ecotec engine with an engine displacement of 2.0 L was used in this paper. Premium grade indolene fuel was used for all experiments. Modifications to the engine for HCCI combustion included an increased geometric compression ratio of 11.25:1, and shorter duration and lower lift cam profiles to allow for unthrottled operation. An Eaton M24 supercharger was used to boost intake manifold pressure to approximately 1.1 bar. The relative air–fuel ratio λ varied between $1 \rightarrow 1.3$. The spark was left on to prevent fouling and was fixed at 40 °CA after top dead center (aTDC). In-cylinder pressure was sampled for real-time estimation of combustion features and for offline pressure trace analysis [4], [12], [13]. The control strategies were implemented using C and MATLAB code and were tested in real-time using an ETAS ES910 rapid prototyping module. The module uses an 800 MHz Freescale PowerQUICC III MPC8548 processor with 512 MB of RAM.

The primary performance output of the system is combustion phasing or timing, which is quantified by the location of θ_{50} or the engine crank angle at which 50% of the total heat release occurs. The other important output is the indicated mean effective pressure (IMEP), which is indicative of the work output of the engine. The actuators available for control are the exhaust valve closing timing (u_{evc}), the fuel injection timing (u_{soi}) and the fuel injection mass (m_f^{inj}). The exhaust cam position affects the magnitude of the retained exhaust gases, and hence controls the dynamic couplings between engine cycles. The common cam phasing actuator for the engine keeps the valve lift and duration constant. Intake and exhaust cams can be actuated independently. The start of fuel injection timing (u_{soi}) is controlled within the NVO region to modulate various thermal and chemical effects that influence

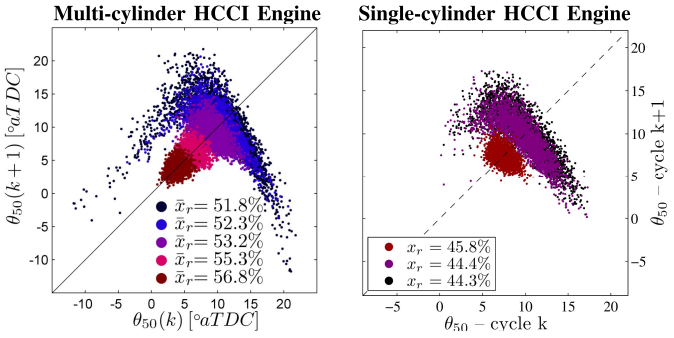

Fig. 4. Return maps from both multicylinder and single-cylinder HCCI engines of measured θ_{50} for operating conditions that differ only in the value of NVO. Smaller NVO values are associated with lower residual gas fractions, later phasing, and high CV. Single cylinder data is taken from [17].

combustion phasing. Fuel mass has a large influence on engine load in HCCI combustion and is scheduled off a look-up table based on desired IMEP. The fuel injection mass and timing can be controlled independently from cylinder to cylinder. The intake cam position mainly affects air flow into the engine and is kept fixed throughout these experiments. The engine speed (ω) is externally specified by the engine dynamometer. Intake and exhaust manifold pressures and temperatures are measured, but not controlled.

III. CV in HCCI

It is well established in [4], [11], [13], [19], [27], and [28] that late phasing HCCI combustion dynamics are qualitatively different from the dynamics seen at early to mid combustion phasings. Experimentally observed CV, as measured by variance of θ_{50}, increases significantly after a certain threshold value of θ_{50}, while combustion stability as well as efficiency drop sharply soon after this threshold. This threshold value ($\theta_{50}^{\text{thresh}}$) varies with engine load and speed and divides the HCCI operation into two dynamically distinct regions—a late phasing high CV region and a normal phasing stable region.

Characterizing and understanding this increased θ_{50} CV is important as steady-state controllers designed to regulate combustion phasing in the late phasing high CV region have been shown to be destabilizing in the normal phasing stable regions and vice-versa [14], [15], [19]. The controller must know the current nature of the combustion dynamics while determining the control input to be applied in the next cycle. This is especially important during HCCI transitions, as transient combustion phasing variation can cause the cylinder combustion to switch between the high CV and low CV regions, even if the two steady-state end points of the transition exist in the stable low CV region. Incorrectly determining the nature of combustion limits the magnitude of transitions possible.

The onset of the high CV region is depicted in Fig. 4 for both single cylinder and multicylinder HCCI engines. The θ_{50} return maps in Fig. 4 are recorded at the same load and speed and only vary in the value of NVO. Several thousand cycles of data were recorded at various steady-state points. The return maps depict couplings between cycles by representing how the value of θ_{50} at cycle (k) depends on the value of θ_{50} at cycle ($k-1$). A return map that is tightly clustered around

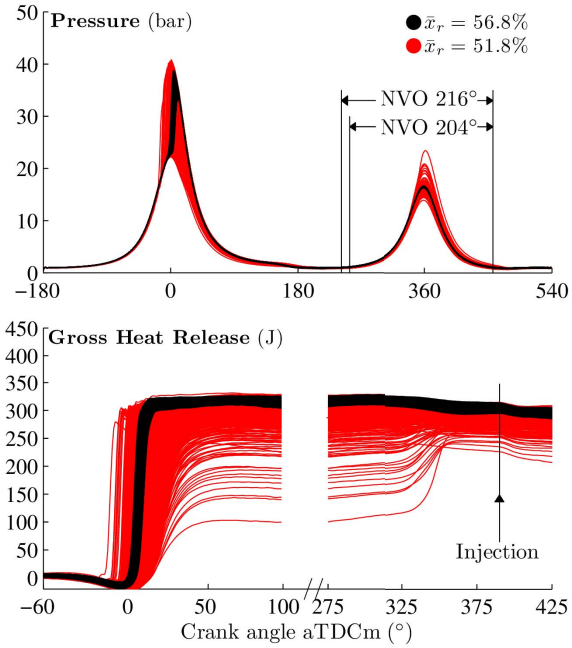

Fig. 5. Comparison of pressure and gross heat release traces for a low CV and high CV NVO heat release and unburned fuel for late-phasing HCCI.

the mean on the diagonal suggests low CV system dynamics that have been perturbed by noise, while a return map with a distinct shape suggests deterministic relationships between cycles. Fig. 4 shows that the level of CV increases sharply as the NVO is reduced, and θ_{50} is phased later.

A. Unburned Fuel Dynamics as the Primary Cause of High CV

In low-order control-oriented HCCI models [11], [14], [15], [19], the high CV dynamic behavior at late phasings manifests itself as a negative discrete eigenvalue, which is associated with oscillatory dynamics. Researchers differ on the physical explanation for this negative eigenvalue. Chiang and Stefanopoulou [11] demonstrated that a single temperature state can model the existence of multiple equilibria for rebreathing HCCI through a bowl-shaped T_{ivc}–T_{bd} combustion curve. Later, similar analysis was performed in [19] for recompression HCCI, where they hypothesize that the negative eigenvalue is caused by an increased heat transfer around TDC.

While heat transfer may be a factor, experimental and modeling works in [16], [17], [27], [29], and [30] show that heat release during the NVO region resulting from the presence of unburned fuel is the primary cause of increased late-phasing oscillations seen in autoignition combustion modes. Through the use of statistical analysis tools in [16] and [17], it is shown that incomplete combustion during the main combustion event leads to a secondary heat release during the NVO region that sets up the characteristic late–early–late oscillatory behavior seen in both single-cylinder and multicylinder recompression HCCI engines.

A experimental demonstration of the heat release during NVO due to unburned fuel is observed in Fig. 5, which compares the measured pressure traces and heat release analysis

results for two steady state HCCI operating points. These points only differ in the u_{evc} position, with all other actuators kept constant. Fig. 5 presents 3000 engine cycles of data measured at each operating point. The point with the later u_{evc} has a lower estimated residual gas fraction. The resulting lower charge temperatures and later combustion phasings push this point into the high CV region. Cycles with extremely late θ_{50} demonstrate poor main combustion efficiency and low heat release during main combustion. These specific engine cycles show clearly observable heat release behavior in the NVO region that occurs before the fuel injection event, which demonstrates that unburned fuel in the recycled charge both exists and participates in exothermic reactions. The increased temperature of the retained charge leads to a very early phasing for the subsequent combustion, thus setting up an oscillatory late–early–late behavior. For more detailed analysis, refer to [4] and [13].

B. Characterizing the Onset of High CV

Predicting the presence of unburned fuel mass after main combustion is used as a proxy for determining the nature of the combustion. Heat release analysis results from the multicylinder HCCI engine at different fueling levels are presented in Fig. 6. In Fig. 6, estimated combustion efficiency is plotted versus θ_{50} and estimated peak combustion temperature. Tens of thousands of engine cycles are recorded at several different values of u_{soi} and u_{evc} to get a large spread in θ_{50}. The combustion efficiency drops from its nominal value at later phasings, suggesting incomplete combustion. This leads to increased amounts of unburned fuel and the onset of CV.

The onset of high CV occurs at earlier combustion phasings for lower m_f^{inj} values (the single cylinder experiments of Fig. 2). This effect can be explained by the peak combustion temperature in the cylinder falling below 1500 K, a temperature threshold below which the *CO* to CO_2 conversion efficiency is known to drop significantly [31]. At lower m_f^{inj} values, this threshold temperature is reached at earlier combustion phasings, and hence the onset of CV occurs at earlier θ_{50} values. Note that temperatures presented in Fig. 6 are estimates from the heat release analysis, as the actual in-cylinder temperature can typically not be measured using near-production engine hardware. Further, the estimated temperature is a mean cylinder temperature that averages temperature gradients caused by phenomena such as inhomogeneous mixing and increased heat transfer near cylinder walls and crevices. These uncertainties, assumptions, and noise lead to a spread in the estimated peak combustion temperature threshold.

The data fits for combustion efficiency (η_m) presented in Fig. 6 are sigmoids, of the following form:

$$\eta_m(k) = \frac{\beta_1\left(m_f^{\text{inj}}\right)}{1+\exp\left\{\frac{\theta_{50}(k)-\beta_2\left(m_f^{\text{inj}}\right)}{\beta_3}\right\}} \tag{1}$$

$$\beta_1\left(m_f^{\text{inj}}\right) = \beta_{1a} + \beta_{1b} m_f^{\text{inj}} \tag{2}$$

$$\beta_2\left(m_f^{\text{inj}}\right) = \beta_{2a} + \beta_{2b} m_f^{\text{inj}} \tag{3}$$

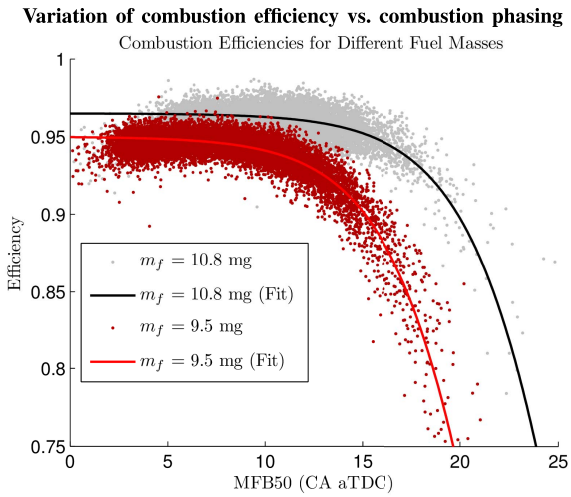

Fig. 6. Combustion efficiencies at two fueling levels are plotted versus combustion phasing and peak cylinder temperature. Low peak combustion temperature $\Longrightarrow$ low combustion efficiency $\Longrightarrow$ significant amounts of unburned recycled fuel. The curve fits are sigmoids (1). Heat release analysis [4], [13] is used to determine the combustion efficiency.

where β_x, $x \in \{1a, 1b, 2a, 2b, 3\}$ are obtained from experimental data, and can be obtained in Fig. 6. The shape parameter β_3 is kept constant for all fueling levels. The coefficients are fitted using a least squares analysis.

IV. HCCI Combustion Model and Validation

The trapped residual gas fraction in recompression HCCI can be as high as 70%, which leads to significant intercycle couplings that need to be modeled accurately by the control-oriented model. The discrete-time model presented here extends the HCCI models developed for operating regimes with near-complete combustion and low cycle-to-cycle variability in [8]–[10]. In general, combustion is to be maintained in these regions for driveability and fuel economy. However, predicting HCCI combustion dynamics in regions of high CV is extremely important when operating near regions of instability or during transient operation. The novelty of the work presented here is that the model is, to the best of the authors' knowledge, the first HCCI combustion model that predicts the nature and magnitude of CV in both low CV and high CV regions.

The interactions between engine cycles are modeled through thermal, composition, and chemical dynamics, via the temperature of the blowdown gases ($T_{\rm bd}$), burned gas fraction of the blowdown gases ($b_{\rm bd}$), and unburned fuel ($m_f^{\rm ub}$) states, respectively. The burned gas fraction is the mass fraction of cylinder charge that is neither fuel nor air. The blowdown process refers to the rapid equalization of the cylinder pressure and the exhaust runner pressure just after exhaust valve opening ($u_{\rm evo}$). The sampling period of the model is one engine cycle.

The HCCI model from [8]–[10] is presented in Section IV-A. This model is valid in the low CV dynamical region. The model is then augmented with unburned fuel state and recompression heat release in Section IV-B.

A. Model Equations for Low CV Operating Region

The nonlinear two-state HCCI combustion model state update equations from [8]–[10] are summarized as follows:

$$T_{\rm bd}(k+1) = \left(\frac{p_{\rm ivc}}{p_{\rm em}}\right)^{\frac{1-n_c}{n_c}} \times \left[1 + \frac{\eta_m\, q_{\rm lhv} R m_f^{\rm inj}}{c_v\, p_{\rm ivc} V_{\rm ivc}} \left(\frac{V_{50}}{V_{\rm ivc}}\right)^{n_c-1}\right]^{\frac{1}{n_c}} T_{\rm ivc}$$

$$b_{\rm bd}(k+1) = \frac{(\,{\rm AFR}_s + 1)\, R m_f^{\rm inj}}{p_{\rm ivc} V_{\rm ivc}} T_{\rm ivc} + x_r b_{\rm bd}(k) \tag{4}$$

where the residual gas fraction (x_r), the specific heat (c_v), and the temperature at IVC ($T_{\rm ivc}$) are given by

$$T_{\rm ivc} = x_r \alpha_2 \left(\frac{V_{\rm evc}}{V_{\rm ivc}}\right)^{n_c-1} T_{\rm bd}(k) + (1 - x_r)\, T_{\rm im} \tag{5}$$

$$x_r = 1 - (a_1 + a_2 u_{\rm evc}) \left(\frac{p_{\rm im}}{p_{\rm em}}\right)^{a_3} \omega^{a_5} T_{\rm bd}(k)^{a_4} \tag{6}$$

$$c_v = 1 + \alpha_1 x_r b_{\rm bd}(k) \tag{7}$$

$$T_{\rm evc} = c_e T_{\rm bd}(k). \tag{8}$$

Here p_x, T_x, and V_x are pressures, volumes, and temperatures, respectively, at the specified engine event x. In particular, V_{50} is the in-cylinder volume at θ_{50}. The model parameters c_e, α_i, and a_j ($i \in \{1, 2\}$, $j \in \{1, \ldots, 5\}$) are tuned using steady-state experimental data. The polytropic exponent (n_c), lower heating value ($q_{\rm lhv}$), stoichiometric air–fuel ratio ($\,{\rm AFR}_s$), and gas constant (R) are fixed constants. In Section IV-B, $T_{\rm evc}$ will be augmented with recompression heat release.

The autoignition process is approximated as a single-step global reaction with an Arrhenius-type reaction rate [32], using a fixed activation temperature ($B = E_a/R_u$) and preexponential factor (A). The integration is carried out until the Arrhenius threshold ($K_{\rm th}$) is hit at the start of combustion ($\theta_{\rm soc}$). Injecting earlier in the recompression region advances phasing approximately linearly and is thus modeled to linearly reduce the integration threshold. The following are solved for $\theta_{\rm soc}$ and θ_{50}:

$$K_{\rm th}(u_{\rm soi}) = k_0 - u_{\rm soi} = \int_{u_{\rm ivc}}^{\theta_{\rm soc}} \frac{A}{\omega} p_c(\theta)^{n_p} \exp\left(\frac{B}{T_c(\theta)}\right) {\rm d}\theta \tag{9}$$

$$\theta_{50} = \gamma_1 \theta_{\rm soc} + \gamma_0. \tag{10}$$

Here k_0, n_p, A, B, γ_0, and γ_1 are model parameters. The pressure (p_c) and temperature (T_c) of the cylinder charge are given by polytropic compression. In this paper, $\theta_{\rm soc}$ is considered to be θ_{02}, the engine crank angle at which 2% of the total heat release occurs. For more details, please refer to [8]–[10].

B. Extension to the High CV Operating Regime

As discussed in Section III, the onset of high CV in HCCI combustion is caused by the presence of significant amounts of unburned fuel after main combustion, which leads to heat release in the NVO region. The unburned fuel after main combustion ($m_f^{\rm ub}$) and the residual mass of fuel that is recycled in the recompression region ($m_f^{\rm res}$) are calculated as follows:

$$m_f^{\rm ub}(k+1) = (1 - \eta_m(k))\, m_f^{\rm inj}(k) \tag{11}$$

$$m_f^{\rm res}(k) = x_r m_f^{\rm ub}(k). \tag{12}$$

The unburned fuel is assumed to be uniformly distributed in the exhaust gases. It is partially exhausted during the exhaust valve open period, while an x_r fraction of it is retained in the NVO region. The combustion efficiency is derived in (1).

Some of the recycled fuel, given by the fraction η_r, exothermically reacts during recompression. The resultant heat release is modeled by adding a temperature rise due to NVO heat release ($\Delta T_{\rm NVO,HR}$) at $u_{\rm evc}$

$$\begin{aligned} T_{\rm evc}(k) &= c_e T_{\rm bd}(k) + \Delta T_{\rm NVO,HR} \\ &= c_e T_{\rm bd}(k) + \frac{\eta_r\, q_{\rm lhv}}{c_v m_c^{\rm nvo}} m_f^{\rm res}(k) \\ &= c_e T_{\rm bd}(k) + \frac{\eta_r\, q_{\rm lhv}}{c_v\, p_{\rm em} V_{\rm evc}} T_{\rm evc} m_f^{\rm res}(k) \\ &= c_e T_{\rm bd}(k) \left(1 + \eta_r \mu \frac{x_r m_f^{\rm ub}(k)}{p_{\rm em} V_{\rm evc}}\right). \end{aligned} \tag{13}$$

Here μ is the single scaling parameter that is tuned to match the system dynamics and the high CV statistics. The mass of charge in the NVO region ($m_c^{\rm nvo}$) is evaluated using the ideal gas law at $u_{\rm evc}$. The efficiency of burn during NVO is assumed to be 100%, which is supported by the vast majority of the heat release traces recorded on the experimental multicylinder engine (Fig. 5). Note however that single cylinder HCCI experiments suggest that η_r can be less than 100% for other experimental setups [4]. This is an important assumption as it simplifies the fuel mass balance and recompression heat release equations. Further, it means that the unburned fuel mass state ($m_f^{\rm ub}$) is merely a unit delay that facilitates information exchange between cycles. This new state has no dynamics, and it shows up in pole-zero maps as a pole at origin.

C. Model Validation Results

Model coefficients were determined using a least squares optimization process, with hand-tuning of a single parameter (μ). Experimental data and heat release analysis results were compared with model predictions, with the model being

evaluated for the following criteria:

1) prediction of the onset of high CV during an actuator sweep, where one actuator (say u_{evc}) is varied while keeping all other actuators constant;
2) prediction of mean θ_{50} in both low and high CV regions.

1) Return Maps Comparison During u_{evc} Sweep: The HCCI combustion demonstrates a nonzero level of variability, even if all control actuators are kept fixed. An underlying level of stochastic disturbances and measurement noise always exist, even in the low CV dynamical region. In addition to the ignition event itself being stochastic, at steady state conditions, the air flow through the cylinders can vary slightly from cycle to cycle, which results in variations in mass of residuals, the charge temperature, and the charge composition. Indeed, these variations are more pronounced in the high CV region, where the combustion dynamics are closer to instability and hence more sensitive to external disturbances. These stochastic disturbances can be simulated by augmenting the residual gas fraction regression given by (6) with an additive factor (Δx_r) as follows:

$$x_r(k) = \left[1-(\alpha_0+\alpha_1 u_{\text{evc}})\Pi^{\alpha_2} T_{\text{bd}}(k)^{\alpha_3}\omega(k)^{\alpha_4}\right] + \Delta x_r. \quad (14)$$

Following the methodology outlined in [4] and [17], Δx_r is modeled to be zero-mean Gaussian noise.

Figs. 7 and 8 compare u_{evc} sweeps at two fueling levels. The u_{evc} is swept in five steps from an early position to a late position, and consequently the nature of the combustion transitions from low CV to high CV. The standard deviation of the Gaussian x_r additive noise was tuned so that the standard deviations of the experimental and modeled θ_{50} plots are similar. Each experiment and simulation was run for 3000 engine cycles to allow the test to be statistically significant, and to allow deterministic patterns to emerge.

Figs. 7 and 8 show that the model can successfully predict the qualitative shape of the return maps, as well as the mean θ_{50}, as the combustion transitions into the high CV dynamical region. Note that the qualitative shape, and not the actual time series, of the modeled and experimental θ_{50} are compared. This is because the actual time series of disturbances to the experiments are unknown. For early values of u_{evc}, both experimentally measured and model predicted θ_{50} return maps resemble Gaussian distributions. As u_{evc} is phased later, the increasing mass of unburned fuel sets up increased variability in the modeled θ_{50} that evolves in deterministically similar patterns to those observed in the measurements.

2) Onset of High CV Dynamics: The transition from low CV to high CV dynamics can be visualized in Fig. 9, where the nonlinear CV model is linearized at each u_{evc} level, and the pole locations are plotted. During this sweep, all other control actuators are held constant. As u_{evc} is swept from its early position (here 241.1 °CA aTDC) to its late position (here 252 °CA aTDC), the discrete temperature eigenvalue moves from the right half plane to the left half plane. This clearly demonstrates how and when the nature of the dynamic response switches from damped to oscillatory. The location of the composition eigenvalue does not move much. The third

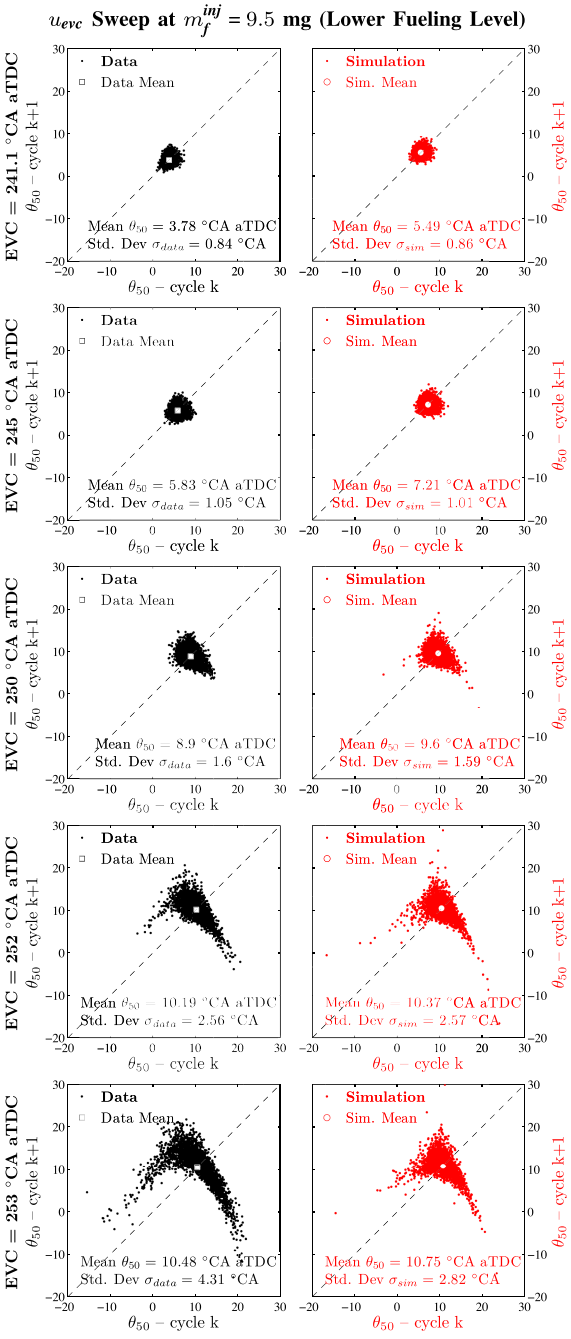

Fig. 7. Comparison of measured (*black*) and simulated (*red*) combustion phasing (θ_{50}) return maps for u_{evc} sweeps at $m_f^{\text{inj}} = 9.5$ mg. Each simulation consists of 3000 engine cycles. The value of u_{soi} is kept constant at 330 °CA bTDC. The onset of high CV conditions at late phasing can be seen.

eigenvalue is fixed at origin, as the m_f^{ub} state is used solely for information exchange between engine cycles, and as such is a unit delay with no dynamics.

The model predictions are also visualized in the return maps plotted in Fig. 9 (right). Here the nonlinear model is run at the five operating points that comprise the u_{evc} sweep. Variability is introduced via Gaussian x_r additive noise, as in (14). Later u_{evc} values result in lower residuals, oscillatory dynamics, and increased variability.

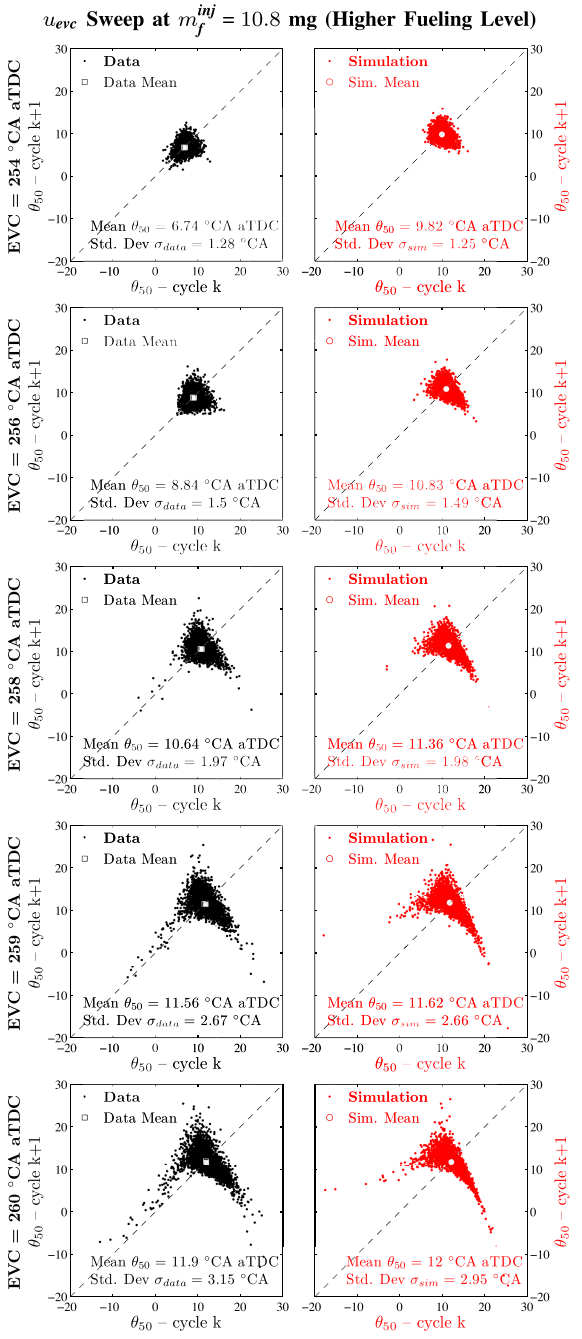

Fig. 8. Comparison of measured (*black*) and simulated (*red*) combustion phasing (θ_{50}) return maps for u_{evc} sweeps at $m_f^{\text{inj}} = 10.8$ mg. Each simulation consists of 3000 engine cycles. The value of u_{soi} is kept constant at 330 °CA bTDC. The onset of high CV conditions at late phasing can be seen.

D. Scope and Limitation of CV Model

The location of the onset of high CV occurs when the nature of the CV qualitatively transitions from stable and damped to oscillatory. In terms of the model just described, it occurs when the temperature pole transitions to the negative real axis. This location of onset of high CV is very sensitive to environmental conditions and engine ageing. Results can vary from day to day. Hence specifying the exact θ_{50} at which the onset occurs is of limited use. This makes modeling the onset and nature of CV a difficult task. In the current application, all validation and parameterization data were taken in a single engine experiment, so that the effect of engine ageing was minimized.

Slowly adapting the value of the scaling parameter (μ) over time can be implemented in future work to counteract the effects of engine ageing.

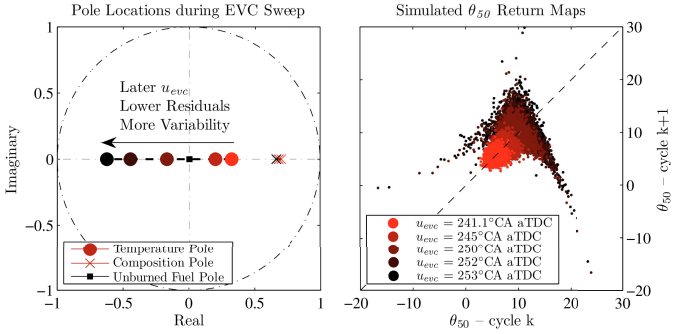

Fig. 9. A u_{evc} actuator sweep at $m_f^{\text{inj}} = 9.5$ mg is visualized through the location of the poles of the linearized CV model (left), and by comparing return maps of the predicted θ_{50} at each operating point. Later u_{evc} values result in lower residuals, oscillatory dynamics, and increased variability.

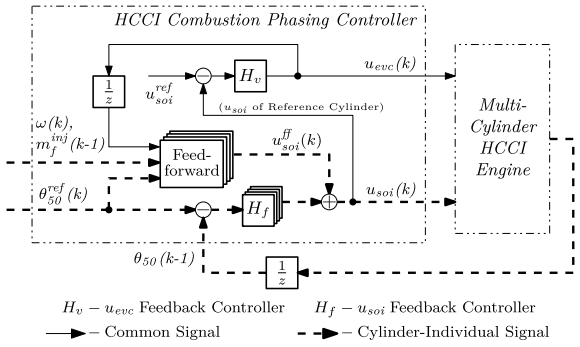

Fig. 10. Controller architecture. Two inputs u_{soi} and u_{evc} in a mid-ranging feedback configuration, with a model-based feedforward for u_{soi}.

V. Controller Design

The controller outlined in Fig. 3 tracks the combustion phasing (θ_{50}) of the four cylinders to their desired set points (θ_{50}^{ref}) during both transient and steady state HCCI operation. During an HCCI transition, changes in engine load (IMEP), engine speed (ω), and desired combustion phasing (θ_{50}^{ref}) are externally specified. Four values of u_{soi} (one for each cylinder) and a single value of u_{evc} (common for the engine) are available for combustion phasing control. The m_f^{inj} injected in each cylinder is specified as a function of the desired engine load and is not used for θ_{50} tracking control. Equal masses of fuel are commanded in each cylinder.

An overview of the controller is presented in Fig. 10. The feedback loop consists of two PI controllers arranged in a mid-ranging control configuration. Mid ranging is a process control technique in which a coarse actuator and a fine actuator are coordinated to control a single feedback output [33]. This two-input single-output control technique is selected considering the relative bandwidths and control authorities of the u_{soi}

and u_{evc} actuators. The fine actuator u_{soi} is used to track desired θ_{50}^{ref}, while the coarse actuator u_{evc} is used over a larger time scale to return u_{soi} to its nominal setpoint, about which it has sufficient controller authority in both directions. This architecture has been used in HCCI engine control applications [34], [35]. The controller is augmented with a u_{soi} feedforward component to improve transient performance. Antiwindup schemes are implemented in the controller to help deal with both u_{soi} and u_{evc} actuator saturation.

This controller architecture (midranging with u_{soi} feedforward) has been used by the authors in previously published HCCI control papers. In [9] and [10], this architecture was used to design the baseline controller, which did not perform well during large load transitions, even leading to engine misfire. The controller performance is significantly improved here through two contributions—nonlinear model-inversion-based u_{soi} feedforward and a gain scheduled u_{soi} feedback that distinguishes whether the cylinder combustion is in the high CV or low CV dynamic region.

A. Nonlinear Model Inversion Based u_{soi} Feedforward

HCCI transitions involving changes in desired load, engine speed, or θ_{50}^{ref} can cause significant θ_{50} variations if not correctly compensated for. The feedback loop, by definition, cannot react until at least one engine cycle after these disturbances occur. In extreme cases, large transitions can cause the engine to misfire. Hence accurate feedforward is needed to improve transient θ_{50} tracking performance during HCCI transitions.

The feedforward u_{soi} component (u_{soi}^{ff}) is designed to drive θ_{50} to θ_{50}^{ref} at steady state, if all other inputs to the system stay constant. It is computed by inverting the nonlinear control-oriented model developed in Section IV. Theoretically this provides perfect θ_{50} tracking performance at steady state, in the absence of modeling error or plant ageing.

1) Improvement Over Previous Work: In the baseline control strategy presented in [9] and [10], u_{soi}^{ff} is determined by inverting the model linearized around a typical operating point. This linearization approximation introduces errors that reduce the accuracy of u_{soi}^{ff}, especially if the system is far away from the linearization point. To compensate for these errors, the controller relies more heavily on the feedback u_{soi} component, which reduces the utility of the feedforward during transients. The control strategy presented here improves the accuracy of the model-based feedforward by inverting the nonlinear model. This avoids errors caused by the linearization approximation.

2) Inverting Nonlinear State Update Equations: The nonlinear model is inverted at steady state conditions, i.e., $x(k+1) = x(k) = \overline{x} = [\overline{T}_{\text{bd}}, \overline{b}_{\text{bd}}]^T$, with the desired output combustion phasing $\theta_{50} = \theta_{50}^{\text{ref}}$. The system equations presented in Section IV-A can be rewritten as

$$\overline{T}_{\text{bd}} = \left(\frac{p_{\text{ivc}}}{p_{\text{em}}}\right)^{\frac{1-n_c}{n_c}} \left[1 + \frac{\eta_m\, q_{\text{lhv}} R m_f^{\text{inj}}}{c_v\, p_{\text{ivc}} V_{\text{ivc}}} \left(\frac{V_{\overline{50}}}{V_{\text{ivc}}}\right)^{n_c-1}\right]^{\frac{1}{n_c}} \overline{T}_{\text{ivc}} \tag{15}$$

$$\overline{b}_{\text{bd}} = \frac{(\text{AFR}_s + 1)\, R m_f^{\text{inj}}}{p_{\text{ivc}} V_{\text{ivc}}\,(1 - x_r)} \overline{T}_{\text{ivc}} \tag{16}$$

$$x_r = 1 - (a_1 + a_2 u_{\text{evc}}) \left(\frac{p_{\text{im}}}{p_{\text{em}}}\right)^{a_3} \omega^{a_5} \overline{T}_{\text{bd}}^{a_4} \tag{17}$$

$$c_v = 1 + \alpha_1 x_r \overline{b}_{\text{bd}} \tag{18}$$

$$\overline{T}_{\text{ivc}} = x_r \alpha_2 \left(\frac{V_{\text{evc}}}{V_{\text{ivc}}}\right)^{n_c-1} \overline{T}_{\text{bd}} + (1 - x_r)\, T_{\text{im}}, \tag{19}$$

where $\overline{T}_{\text{ivc}}$ is the temperature at u_{ivc} at steady state, and $V_{\overline{50}}$ is the cylinder volume at the desired θ_{50}^{ref}. The system of equations (15)–(19) is solved using fixed point iteration. The number of iterations required depends on the convergence tolerance desired. The resulting value of $\overline{T}_{\text{ivc}}$ is used with θ_{50}^{ref} in (9) and (10) to determine the desired u_{soi}^{ff}.

B. High CV Capable Gain Scheduled u_{soi} Feedback

In the baseline control strategy presented in [9] and [10], $u_{\text{soi}}^{\text{fb}}$ is generated using fixed gains that are appropriate for the low CV dynamical region. As will be shown in this section, this is not optimal near the limits of the HCCI operating region or during transients.

1) Controller Design: The gain scheduled u_{soi} feedback determines if the cylinder combustion is in either the low CV or the high CV region, and then applies the appropriate proportional gain. Combustion is determined to be in the high CV oscillatory region if low combustion efficiency, and thus the existence of a significant amount of unburned fuel, is predicted. Based on the discussion in Section III, this is modeled to happen if the combustion phasing θ_{50} is later than a threshold combustion phasing value ($\theta_{50}^{\text{thresh}}$). Further, $\theta_{50}^{\text{thresh}}$ varies with engine load, which is represented here by m_f^{inj}.

The proportional gain K_p^{soi} of the u_{soi} PI controller (H_f in Fig. 10) is gain scheduled, based on whether the controller decides that the system is in the high CV or low CV region

$$K_p^{\text{soi}} = \begin{cases} K_{p,\text{lowcv}}^{\text{soi}}, & \text{if } \theta_{50}(k) \le \theta_{50}^{\text{thresh}}(m_f^{\text{inj}}) \\ K_{p,\text{highcv}}^{\text{soi}}, & \text{if } \theta_{50}(k) > \theta_{50}^{\text{thresh}}(m_f^{\text{inj}}). \end{cases} \tag{20}$$

The values of the proportional gains ($K_{p,\text{lowcv}}^{\text{soi}}$ and $K_{p,\text{highcv}}^{\text{soi}}$) were determined from prior control design work done for the low CV region in [10] and for the high CV region in [14]. $K_{p,\text{lowcv}}^{\text{soi}}$ was determined through a nonlinear least-squares optimization of the closed-loop system in simulation, while $K_{p,\text{highcv}}^{\text{soi}}$ was determined through a pole placement analysis using the nonlinear high CV model. It is important to note that $K_{p,\text{lowcv}}^{\text{soi}}$ and $K_{p,\text{highcv}}^{\text{soi}}$ have opposite signs, due to the presence of the negative eigenvalue in the high CV region. The integral gain K_i^{soi} of the u_{soi} PI controller was kept constant. The coarse actuator u_{evc} is controlled by a slow integrator (H_v in Fig. 10) over a larger time scale to return u_{soi} to its setpoint. The specific value of $\theta_{50}^{\text{thresh}}$ (m_f^{inj}) will be stated in each of the experimental results presented in Section VI.

A similar switching concept is used in the controller design by Liao *et al.* [19] and is used to track steps in desired θ_{50}^{ref} at a single load/speed HCCI operating point. However, as discussed in Section III, recompression heat release due

TABLE I
LINEARIZATION OPERATING POINTS FOR THE HCCI MODEL

Quantity	Low CV Oper. Point	High CV Oper. Point
u_{evc}	241.1 °CA aTDC	252 °CA aTDC
m_f^{inj}	9.51 mg/cycle	9.51 mg/cycle
u_{soi}	330 °CA bTDC	330 °CA bTDC
ω	1800 rpm	1800 rpm
θ_{50}	5.48 °CA aTDC	10.89 °CA aTDC
Pole Locations	{0.320, 0.696}	{-0.446, 0.658}

to unburned fuel, and not increased heat transfer around TDC, is the primary physical phenomenon that determines the magnitude and dynamic evolution of highly variable late phasing HCCI. A more accurate understanding of the underlying physics helps design controllers that work over larger operating ranges.

2) Closed Loop Step Responses of Controller: The HCCI model is linearized at a low CV and a high CV operating point, as specified in Table I. As expected, the open loop plant poles at the low CV operating point are damped and stable, while those at the high CV operating point are oscillatory. The closed-loop pole locations of three different plant and controller combinations that correspond to the fixed gain and the gain scheduled controllers are considered, as follows:

1) model linearized at low CV operating point, with $K_p^{\text{soi}} = K_{p,\text{lowcv}}^{\text{soi}}$: $\{0.9681, 0.8903, 0.6930, 0.3054, 0, -0.0127\}$;
2) model linearized at high CV operating point, with $K_p^{\text{soi}} = K_{p,\text{lowcv}}^{\text{soi}}$: $\{0.9568, 0.9187, 0.6502, 0.0670, 0, -0.6946\}$;
3) model linearized at high CV operating point, with $K_p^{\text{soi}} = K_{p,\text{highcv}}^{\text{soi}}$: $\{0.9572, 0.8974, 0.6318, 0.0196 \pm 0.4907i, 0\}$.

From this list, it is seen that using fixed gain feedback at high CV operating conditions introduces oscillatory dynamics through the closed-loop pole located on the negative real axis (-0.6946). Using $K_p^{\text{soi}} = K_{p,\text{highcv}}^{\text{soi}}$ instead, as suggested by the gain-scheduled feedback, pulls this closed-loop pole into the right half unit circle. This can be observed in an alternative manner in the closed-loop step responses in Fig. 11. In Fig. 11, the θ_{50} responses of the closed-loop systems to unit steps in m_f^{inj} and θ_{50}^{ref} are compared. It is clearly seen that the responses of the improved controller are stable and nonoscillatory in both low CV and high CV dynamical regions.

Note that stability during switching is not commented on. Switching between individually stable systems does not guarantee stability of the switched system in general. Using the theory of switched linear systems to demonstrate stability of the gain scheduling scheme using linearized plant models is planned for future work. An example of such a stability analysis for a HCCI control strategy is seen in [19].

3) Experimental Validation of Gain Scheduled Feedback: An experimental demonstration of the benefits of the gain scheduled u_{soi} feedback is presented in Fig. 12. Fig. 12 compares the performance of the control architecture presented in Fig. 10 with fixed gain and with gain scheduled u_{soi} feedback for both transient and steady state operation. The θ_{50}

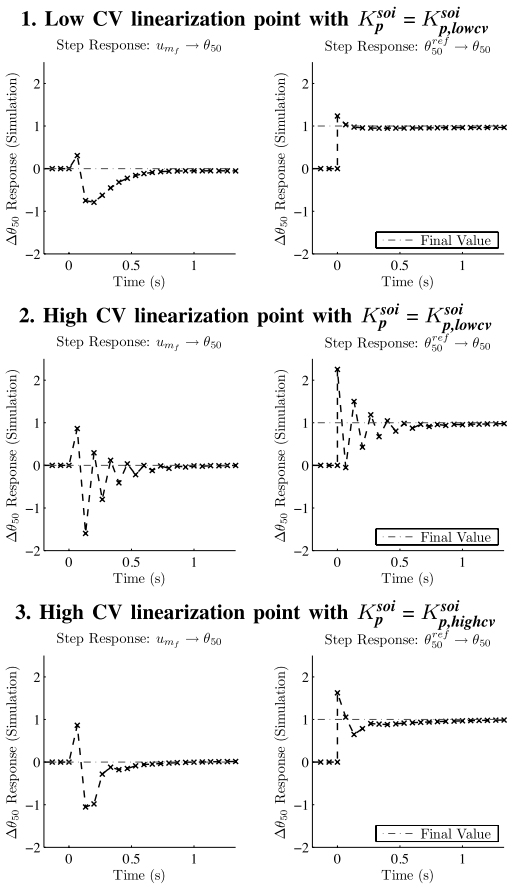

Fig. 11. Simulated step responses for baseline and improved controllers. Using two different K_p^{soi} gains avoids oscillatory response.

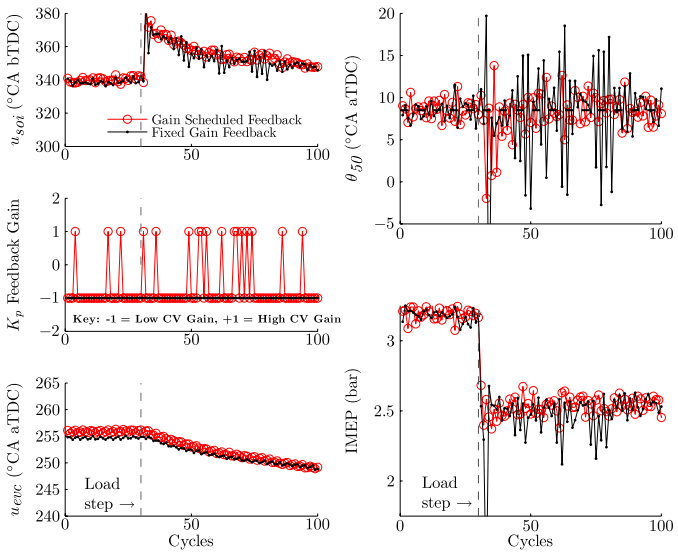

Fig. 12. Comparison of gain scheduled feedback with fixed gain feedback. Transient response to load step down, with $\theta_{50}^{\text{thresh}} = 10$ °CA.

and load tracking performance is compared during a load step down from $m_f^{\text{inj}} = 10.4$ mg to 8.7 mg. The value of $\theta_{50}^{\text{thresh}}$ is 10 °CA aTDC. As can be seen, the initial transient response of the controller with the gain scheduled feedback is significantly smoother. The IMEP steps between the initial and final values

in a single cycle, and an engine misfire is prevented. At the lower load level, the cylinder combustion dynamics enter the high CV oscillatory region, where the fixed gain feedback controller is unable to regulate θ_{50} well. A typical pattern is noted where the magnitude of oscillations are amplified by the controller before returning to the desired value and starting up again. These oscillations are also associated with undesired fluctuations in the torque output. This oscillatory behavior is successfully attenuated by the gain scheduling controller. Note that the gain scheduling controller only switches gains when the value of θ_{50} is later than the desired threshold $\theta_{50}^{\text{thresh}}$.

VI. Load and Speed Transitions

The experimental results in this section demonstrate that the controller can track desired combustion phasing during HCCI transitions similar to those seen during a typical drive cycle. The transitions considered consist of a combination of simultaneously varying engine load (desired IMEP), engine speed, and desired combustion phasing (θ_{50}^{ref}).

First in Section VI-A, good θ_{50}^{ref} regulation performance during load transitions at a fixed engine speed is demonstrated. Results are presented for both tip-in and tip-out behavior. Section VI-B presents control results for simultaneous load and speed transitions. Finally, in Section VI-C, the controller is tested on some select transitions with high load slew rates from an FTP75 drive cycle analysis.

A. Load Transitions at Fixed Engine Speed

Fig. 13 shows control results for two load transitions with engine speed fixed at 1500 revolutions/min. The subfigures on the top and bottom present results for load steps down and up, respectively. The load step down is the more challenging of the two to control, as the significantly reduced charge temperatures can lead to excessively late phasing, high CV, and potential engine misfire. In these transitions, the desired θ_{50}^{ref} and the gain scheduling threshold $\theta_{50}^{\text{thresh}}$ are kept constant.

The fuel mass for the transitions is stepped over a single cycle at time $t = 1$ s. The torques for all four cylinders step smoothly from the initial to the final values without any spikes or dips. Note that the cylinder torques differ due to cylinder-to-cylinder variations in a multicylinder engine. These torque differences can be controlled by varying m_f^{inj} on a cylinder-to-cylinder basis, but in this paper, m_f^{inj} for all cylinders was kept constant. Good θ_{50} regulation performance is observed for all four cylinders. The combustion phasing is regulated to the setpoint of 8.5 °CA aTDC and stays within reasonable bounds during the load transition.

The control inputs u_{soi} and u_{evc} demonstrate typical mid-ranging behavior. As explained in Section V, the initial transient response to load step is controlled by the fine actuator (u_{soi}). The sudden initial jump in the u_{soi} response is driven by the u_{soi} feedforward block, and compensates for the sudden change in charge temperature before any adverse effect on the θ_{50} output can be seen. The coarse actuator (u_{evc}) slowly returns u_{soi} of a reference cylinder, here cylinder 1, back to its nominal setpoint, which is 330 °CA before top dead center (bTDC) in these tests. Note that due to cylinder-to-cylinder

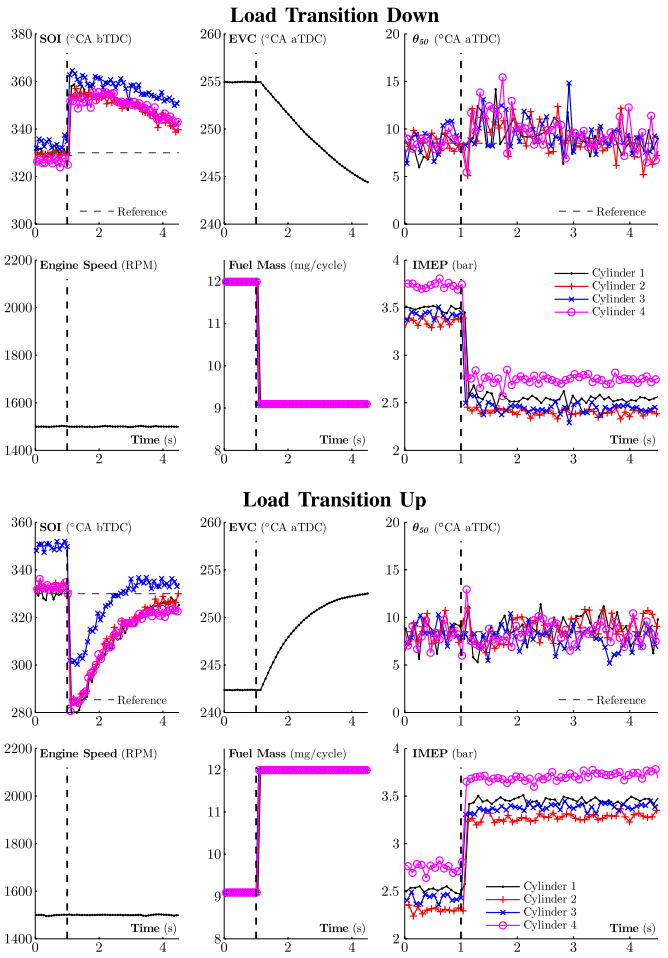

Fig. 13. Load transition at fixed engine speed—θ_{50} regulation during load steps up and down. Note that the u_{soi} actuators are cylinder individual, but there is only a single u_{evc} actuator for the entire engine.

variations in a multicylinder engine, only one of the u_{soi} actuators can be returned to the nominal setpoint. In addition, the u_{soi} actuator is saturated at 280 °CA bTDC to avoid fuel injection while the intake valve is open. In Fig. 13, results are shown for all four cylinders. Henceforth, results for a single cylinder will be presented for clarity.

Load transitions of this magnitude cause the baseline controller in [9] and [10] to fail and cause engine misfires. The proposed solution in the cited works involved the addition of a reference governor that is a model-predictive filter that intelligently slows down the desired load command. The current controller is an improvement as it does not slow down the load command at all. It is able to compensate for the entire step in a single cycle, with a load slew rate of approximately 1 bar/cycle. This quick matching of the driver's desired torque demand improves driveability.

Fig. 14 shows how the measured pressure traces vary before and during a controlled load transition at a fixed engine speed of 1800 revolutions/min. The data plotted in black occurs before the load transition, and the data plotted in red occurs after the load step down. The pressure traces shrink and the peak pressures drop significantly in a single cycle after the transition. The IMEP results confirm that the load drops smoothly from the initial to the final value with no significant

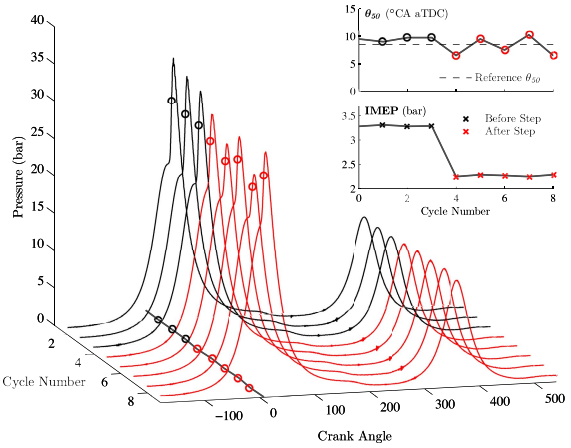

Fig. 14. Pressure traces before and after a load step down at 1800 revolutions/min. The cycle-by-cycle θ_{50} values are plotted on the pressure traces, and are projected onto the x-and y-planes.

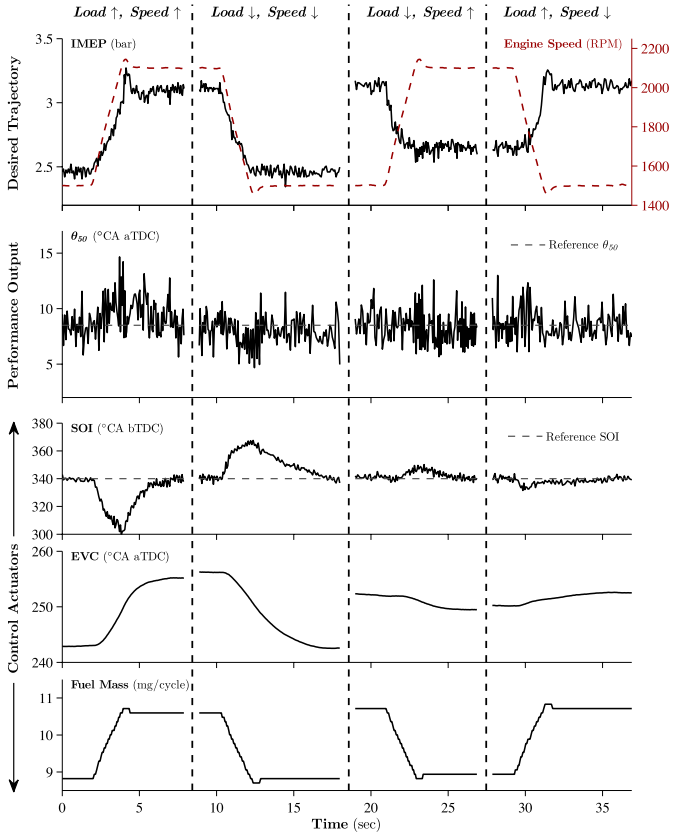

Fig. 15. Simultaneous load and speed transitions—θ_{50} regulation results shown for four combinations of engine load and speed ramps.

oscillations. The θ_{50}^{ref} regulation performance is good, with the measured θ_{50} not deviating significantly from the desired $\theta_{50}^{\text{ref}} = 8.5$ °CA aTDC.

B. Simultaneous Load and Speed Transitions

In this section, θ_{50} regulation results are presented for simultaneous load and speed transitions. Fig. 15 presents control results for all four combinations of the desired engine speed and engine load increasing and decreasing.

TABLE II
SELECT HCCI TRANSITIONS FROM FTP75 DRIVE-CYCLE ANALYSIS

Name	Time (sec)		Speed (RPM)			IMEP (bar)	
	From	To	From	To	Chosen	From	To
Down	1301.9	1302.34	2110	2130	2100	3.46	2.39
Up	533.19	533.39	1790	1800	1800	2.63	3.69

In these transitions, engine speed is varied from 1500 to 2100 revolutions/min and vice-versa. Due to experimental dynamometer restrictions, the engine speed slew rate was fixed and could not be varied. The desired load was commanded to vary at the same rate as the engine speed, as seen from the m_f^{inj} actuator plot. In these transitions, the desired θ_{50}^{ref} and the gain scheduling threshold $\theta_{50}^{\text{thresh}}$ are kept constant.

Fig. 15 shows satisfactory θ_{50}^{ref} regulation performance for all four transitions. Misfires are avoided, and the IMEP response is smooth. As can be seen, the magnitudes of u_{soi} and u_{evc} control efforts are significantly more when the desired load and speed move in the same direction (either both increase or both decrease). When the desired engine speed and load move in opposite directions in the transitions presented, the required controller effort is nearly zero. The open loop responses of θ_{50} to the variations in speed and load cancel each other out. Note that the feedforward component of u_{soi} successfully realizes this and does not deviate from the reference u_{soi} setpoint.

C. HCCI Transitions Seen in FTP75 Drive Cycle Analysis

Finally, the controller is tested on select HCCI transitions from the FTP75 drive-cycle analysis performed in [3]. The FTP75 driving cycle was experimentally performed on a chassis dynamometer by a human driver in a Cadillac CTS car equipped with a 3.6L V6 engine. This is the baseline engine and vehicle configuration that is downsized to the 2.0L I4 multimode combustion engine described in Section II. In [3], the engine torque and speed measurements are appropriately scaled to the new engine configuration, and an analysis of transitions within the HCCI region is performed. That analysis is used in this section to determine the HCCI transitions to test.

1) Selection of the HCCI Transitions to be Tested: The transitions tested on the multicylinder engine are listed in Table II. The HCCI transitions with high load slew rates were selected from FTP75 drive-cycle analysis. The transition named down involves a load (IMEP) decrease from 3.46 to 2.39 bar in 7.5 engine cycles. The engine speed does not vary much, and is chosen to be fixed at 2100 revolutions/min. The transition named up involves a load (IMEP) increase from 2.63 to 3.69 bar in 3 engine cycles. Again, the engine speed does not vary much, and is chosen to be fixed at 1800 revolutions/min.

The engine speed range of the HCCI operating region for the multicylinder engine is between 1500 and 3000 revolutions/min. However, the HCCI combustion model used in this paper is tested for a smaller speed range between 1500 and 2200 revolutions/min, and so the HCCI transitions selected from the FTP75 drive cycle analysis were restricted to this speed range. The engine load range of the

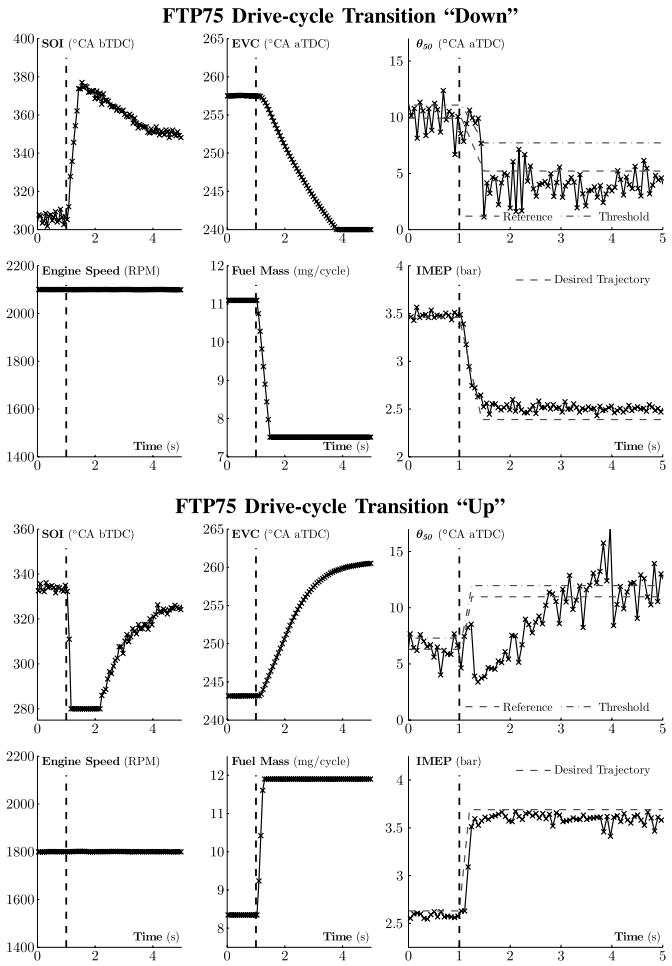

Fig. 16. Load transition at fixed engine speed—θ_{50} regulation during load steps up and down. Note that the $u_{\rm soi}$ actuators are cylinder individual, but there is only a single $u_{\rm evc}$ actuator for the entire engine.

transitions tested is limited by the high and low load range of the HCCI operating map.

2) Discussion of Experimental Results: Fig. 16 presents $\theta_{50}^{\rm ref}$ tracking results for the select HCCI transitions from the FTP75 drive-cycle analysis, as listed in Table II. For both transitions, the IMEP performance output steps smoothly from the initial to the final desired level. Exact steady-state tracking of desired IMEP is not achieved, since in this paper, there is no closed-loop control of IMEP, and $m_f^{\rm inj}$ is scheduled from a predetermined look-up table.

In these transitions, the desired $\theta_{50}^{\rm ref}$ varies as a function of load, and is set later for higher loads. This strategy is more realistic than regulating a constant $\theta_{50}^{\rm ref}$ because it helps reduce high pressure rise rates at higher loads. However, this makes the control problem more challenging, as the transient control requires greater controller effort. As observed in Fig. 16, satisfactory transient $\theta_{50}^{\rm ref}$ tracking is achieved for the transition named down, but there is a large $\theta_{50}^{\rm ref}$ tracking error for about 1 s after the transition named up. However, two seconds after the transition is commanded, satisfactory tracking is achieved. Further, this has no discernable effect on IMEP variability, and hence on driveability.

The initial poor $\theta_{50}^{\rm ref}$ tracking performance in the transition up is due to actuator saturation. The initial transient response to the load variation is almost exclusively provided by the fast actuator $u_{\rm soi}$, which quickly saturates at 280 °CA bTDC. As mentioned earlier, it is saturated at this level to avoid fuel injection while the intake valve is open. While $u_{\rm soi}$ is saturated, the only actuator available for $\theta_{50}^{\rm ref}$ tracking control is the slow $u_{\rm evc}$ actuator that attempts to return $u_{\rm soi}$ away from saturation, and to its nominal value. Poor $\theta_{50}^{\rm ref}$ tracking performance persists while the $u_{\rm soi}$ saturation exists.

Another interesting effect of actuator saturation is seen in the transition named down. Here it is $u_{\rm evc}$ that saturates at 241 °CA aTDC at around $t = 4$ s. This saturation is a hardware limit of the cam phaser. As a result of the architecture of the controller in Fig. 10, this saturation does not affect the $\theta_{50}^{\rm ref}$ tracking performance, but rather prevents $u_{\rm soi}$ from returning to its nominal value. This does not affect the transition under consideration, but does limit subsequent transitions. For example, in this case where $u_{\rm evc}$ is saturated at the early limit, further reductions in load are restricted.

Note that the $K_p^{\rm soi}$ gain scheduling threshold ($\theta_{50}^{\rm thresh}$) is plotted, and varies with load as discussed in Section V-B.

VII. Conclusion

A model-based control strategy is presented to track combustion phasing during HCCI transitions, which include a combination of load, speed, and $\theta_{50}^{\rm ref}$ variations. A low-order control-oriented model is presented that predicts the nature and magnitude of CV in HCCI across both low CV and high CV dynamical regions. The controller uses cylinder individual $u_{\rm soi}$ and $m_f^{\rm inj}$, and cylinder common $u_{\rm evc}$ as control actuators. Novel aspects of the controller include nonlinear model-inversion-based feedforward, and gain scheduled feedback that distinguishes between HCCI combustion regimes demonstrating different dynamic behavior. The occurrence of high CV and low CV dynamic regions is understood through unburned fuel recompression heat release, and this physical understanding is used to improve feedback performance.

The controller is tested on a number of HCCI transitions—including load transitions at fixed engine speeds, combined load and speed transitions, and select transitions from an FTP75 drive-cycle analysis. The controller successfully tracks $\theta_{50}^{\rm ref}$ while transitioning smoothly from one load–speed operating point to the next. As compared with previous control solutions, the current controller does not slow down the desired load command, thus improving driveability. This stable and fast transient control enables the engine to maximize the length of stay in the HCCI region, and hence the efficiency benefit. Actuator saturation can lead to sub-par $\theta_{50}^{\rm ref}$ tracking or $u_{\rm soi}$ mid-ranging performance, but does not affect the IMEP tracking performance. However, this must be kept in mind while implementing the controller on a real engine.

Future work involves extending the validity of the HCCI model to the entire HCCI operating map speed range from 1500 to 3000 revolutions/min. Currently, it is parameterized for approximately half this range. In addition, the model fidelity reduces over time due to engine ageing, which in turn reduces the accuracy of the model-inversion-based feedforward. Adaptive techniques that improve the model and feedforward controller accuracy are currently being experimentally

tested. The model for recompression heat release used here is relatively simple, with a single scaling parameter (μ). A more sophisticated modeling of NVO heat release can be implemented in future work to further improve modeling results. Slowly adapting the value of the scaling parameter over time can be implemented to counteract the effects of engine ageing.

ACKNOWLEDGMENT

The authors would like to thank J. Sterniak and J. Vanier for their assistance with resolving experimental issues.

REFERENCES

[1] M. Yao, Z. Zheng, and H. Liu, "Progress and recent trends in homogeneous charge compression ignition (HCCI) engines," *Prog. Energy Combustion Sci.*, vol. 35, no. 5, pp. 398–437, Oct. 2009.

[2] F. Zhao, T. N. Asmus, D. N. Assanis, J. E. Dec, J. A. Eng, and P. M. Najt, *Homogeneous Charge Compression Ignition (HCCI) Engines—Key Research and Development Issues*. Warrendale, PA, USA: SAE, 2003, p. 94.

[3] S. Nüesch, E. Hellström, L. Jiang, and A. Stefanopoulou, "Influence of transitions between SI and HCCI combustion on driving cycle fuel consumption," in *Proc. Eur. Control Conf.*, Zürich, Switzerland, Jul. 2013, pp. 1976–1981.

[4] E. Hellström *et al.*, "Understanding the dynamic evolution of cyclic variability at the operating limits of HCCI engines with negative valve overlap," *SAE Int. J. Eng.*, vol. 5, no. 3, pp. 995–1008, 2012.

[5] L. Manofsky, J. Vavra, D. Assanis, and A. Babajimopoulos, "Bridging the gap between HCCI and SI: Spark-assisted compression ignition," SAE Int., Washington, DC, USA, Tech. Rep. 2011-01-1179, 2011.

[6] D. J. Rausen, A. G. Stefanopoulou, J.-M. Kang, J. A. Eng, and T.-W. Kuo, "A mean-value model for control of homogeneous charge compression ignition (HCCI) engines," *J. Dyn. Syst., Meas., Control*, vol. 127, no. 3, pp. 355–362, Sep. 2005.

[7] C.-J. Chiang, A. G. Stefanopoulou, and M. Jankovic, "Nonlinear observer-based control of load transitions in homogeneous charge compression ignition engines," *IEEE Trans. Control Syst. Technol.*, vol. 15, no. 3, pp. 438–448, May 2007.

[8] S. Jade, E. Hellström, A. Stefanopoulou, and L. Jiang, "On the influence of composition on the thermally-dominant recompression HCCI combustion dynamics," in *Proc. ASME Dyn. Syst. Contr. Conf. Bath*, 2011, pp. 2–8.

[9] S. Jade, J. Larimore, E. Hellström, L. Jiang, and A. G. Stefanopoulou, "Enabling large load transitions on multicylinder recompression HCCI engines using fuel governors," in *Proc. Amer. Control Conf.*, 2013, pp. 4423–4428.

[10] S. Jade, E. Hellström, J. Larimore, L. Jiang, and A. G. Stefanopoulou, "Reference governor for load control in a multicylinder recompression HCCI engine," *IEEE Trans. Control Syst. Technol.*, vol. 22, no. 4, pp. 1408–1421, Jul. 2014, doi: 10.1109/TCST.2013.2283275.

[11] C.-J. Chiang and A. G. Stefanopoulou, "Stability analysis in homogeneous charge compression ignition (HCCI) engines with high dilution," *IEEE Trans. Control Syst. Technol.*, vol. 15, no. 2, pp. 209–219, Mar. 2007.

[12] J. Larimore, E. Hellström, J. Sterniak, L. Jiang, and A. G. Stefanopoulou, "Experiments and analysis of high cyclic variability at the operational limits of spark-assisted HCCI combustion," in *Proc. Amer. Control Conf.*, Jun. 2012, pp. 2072–2077.

[13] E. Hellström, J. Larimore, A. Stefanopoulou, J. Sterniak, and L. Jiang, "Quantifying cyclic variability in a multicylinder HCCI engine with high residuals," *J. Eng. Gas Turbines Power*, vol. 134, no. 11, p. 112803, 2012.

[14] J. Larimore, E. Hellström, S. Jade, L. Jiang, and A. G. Stefanopoulou, "Controlling combustion phasing variability with fuel injection timing in a multicylinder HCCI engine," in *Proc. Amer. Control Conf.*, Jun. 2013, pp. 4435–4440.

[15] E. Hellström, J. Larimore, S. Jade, A. G. Stefanopoulou, and L. Jiang, "Reducing cyclic variability while regulating combustion phasing in a four-cylinder HCCI engine," *IEEE Trans. Control Syst. Technol.*, vol. 22, no. 3, pp. 1190–1197, May 2014, doi: 10.1109/TCST.2013.2271355.

[16] E. Hellström and A. G. Stefanopoulou, "Modeling cyclic dispersion in autoignition combustion," in *Proc. 50th IEEE Conf. Decision Control Eur. Control Conf.*, Dec. 2011, pp. 6834–6839.

[17] E. Hellström, A. G. Stefanopoulou, and L. Jiang, "Cyclic variability and dynamical instabilities in autoignition engines with high residuals," *IEEE Trans. Control Syst. Technol.*, vol. 21, no. 5, pp. 1527–1536, Sep. 2013.

[18] A. Widd, H.-H. Liao, J. C. Gerdes, P. Tunestål, and R. Johansson, "Hybrid model predictive control of exhaust recompression HCCI," *Asian J. Control*, vol. 16, no. 2, pp. 370–381, Jun. 2013.

[19] H.-H. Liao, A. Widd, N. Ravi, A. F. Jungkunz, J.-M. Kang, and J. C. Gerdes, "Control of recompression HCCI with a three region switching controller," *Control Eng. Pract.*, vol. 21, no. 2, pp. 135–145, 2013.

[20] S. M. Erlien, A. F. Jungkunz, and J. C. Gerdes, "Multi-cylinder HCCI control with cam phaser variable valve actuation using model predictive control," in *Proc. 5th Annu. Dyn. Syst. Control Conf.*, 2012, pp. 1–9.

[21] N. Ravi, H.-H. Liao, A. F. Jungkunz, A. Widd, and J. C. Gerdes, "Model predictive control of HCCI using variable valve actuation and fuel injection," *Control Eng. Pract.*, vol. 20, no. 4, pp. 421–430, 2012.

[22] N. Ravi, H.-H. Liao, A. F. Jungkunz, C.-F. Chang, H. H. Song, and J. C. Gerdes, "Modeling and control of an exhaust recompression HCCI engine using split injection," *J. Dyn. Syst. Meas. Control*, vol. 134, no. 1, pp. 011016-1–011016-12, Jan. 2012.

[23] N. Ravi *et al.*, "Model-based control of HCCI engines using exhaust recompression," *IEEE Trans. Control Syst. Technol.*, vol. 18, no. 6, pp. 1289–1302, Nov. 2010.

[24] G. M. Shaver, J. C. Gerdes, and M. J. Roelle, "Physics-based modeling and control of residual-affected HCCI engines," *J. Dyn. Syst., Meas., Control*, vol. 131, no. 2, pp. 021002-1–021002-12, Feb. 2009.

[25] N. Ravi, M. J. Roelle, and J. C. Gerdes, "Controller-observer implementation for cycle-by-cycle control of an HCCI engine," in *Proc. IMECE*, 2007, pp. 177–185.

[26] J. Willand, R.-G. Nieberding, G. Vent, and C. Enderle, "The knocking syndrome—Its cure and its potential," SAE Int., Washington, DC, USA, Tech. Rep. 982483, 1998.

[27] C. S. Daw, K. D. Edwards, R. M. Wagner, and J. B. Green, Jr., "Modeling cyclic variability in spark-assisted HCCI," *J. Eng. Gas Turbines Power*, vol. 130, no. 5, p. 052801, 2008.

[28] A. Ghazimirsaied, M. Shahbakhti, and C. R. Koch, "HCCI engine combustion phasing prediction using a symbolic-statistics approach," *J. Eng. Gas Turbines Power*, vol. 132, no. 8, p. 082805, 2010.

[29] L. Koopmans, O. Backlund, and I. Denbratt, "Cycle to cycle variations: Their influence on cycle resolved gas temperature and unburned hydrocarbons from a camless gasoline compression ignition engine," SAE Int., Washington, DC, USA, Tech. Rep. 2002-01-0110, 2002.

[30] R. M. Wagner, K. D. Edwards, C. S. Daw, J. B. Green, Jr., and B. G. Bunting, "On the nature of cyclic dispersion in spark assisted HCCI combustion," SAE Int., Washington, DC, USA, Tech. Rep. 2006-01-0418.

[31] M. Sjöberg and J. E. Dec, "An investigation into lowest acceptable combustion temperatures for hydrocarbon fuels in HCCI engines," *Proc. Combustion Inst.*, vol. 30, no. 2, pp. 2719–2726, Jan. 2005.

[32] S. R. Turns, *An Introduction to Combustion: Concepts and Applications* (Mechanical Engineering), 2nd ed. New York, NY, USA: McGraw-Hill, 2000.

[33] B. J. Allison and A. J. Isaksson, "Design and performance of mid-ranging controllers," *J. Process Control*, vol. 8, nos. 5–6, pp. 469–474, 1998.

[34] M. Karlsson, K. Ekholm, P. Strandh, R. Johansson, P. Tunestål, and B. Johansson, "Closed-loop control of combustion phasing in an HCCI engine using VVA and variable EGR," in *Proc. 5th IFAC Symp. Adv. Autom. Control*, 2007, pp. 501–508.

[35] N. Ravi, H.-H. Liao, A. F. Jungkunz, and J. C. Gerdes, "Mid-ranging control of a multi-cylinder HCCI engine using split fuel injection and valve timings," in *Proc. 6th IFAC Symp. Adv. Autom. Control*, 2010, pp. 797–802.

Shyam Jade (S'11) received the bachelor's degree in mechanical engineering from IIT Bombay, Mumbai, India, in 2009, and the master's and Ph.D. degrees in mechanical engineering from the University of Michigan, Ann Arbor, MI, USA, in 2011 and 2014, respectively.

He is currently a Systems Engineer in Systems and Advanced Engineering with Gasoline Systems North America, Robert Bosch LLC, Pittsburgh, PA, USA. His current research interests include modeling and control development for advanced vehicle powertrain systems.

Jacob Larimore (S'11) received the bachelor's degree in mechanical engineering from the Missouri University of Science and Technology, Rolla, MO, USA, in 2009, and the master's and Ph.D. degrees in mechanical engineering from the University of Michigan, Ann Arbor, MI, USA, in 2012 and 2014, respectively.

He is currently a Systems Engineer in Systems and Advanced Engineering with Gasoline Systems North America, Robert Bosch LLC, Pittsburgh, PA, USA. His current research interests include modeling and control of advanced internal combustion engines, and embedded control systems.

Erik Hellström (M'11) received the M.Sc. degree in applied physics and electrical engineering and the Ph.D. degree from Linköping University, Linköping, Sweden, in 2005 and 2010, respectively.

He was a Research Fellow and Research Scientist with the University of Michigan, Ann Arbor, MI, USA, from 2010 to 2013. He is currently a Research Engineer with Ford Research and Advanced Engineering, Dearborn, MI, USA. His current research interests include modeling, control, and optimal control of vehicle powertrains.

Dr. Hellström is a member of the American Society of Mechanical Engineers and the Society of Automotive Engineers. He is currently an Associate Editor of *Control Engineering Practice*.

Anna G. Stefanopoulou (S'93–M'96–SM'05–F'09) was a Technical Specialist with Ford Motor Company, Dearborn, MI, USA, from 1996 to 1997, and an Assistant Professor with the University of California at Santa Barbara, Santa Barbara, CA, USA, from 1998 to 2000. She is currently a Professor of Mechanical Engineering with the University of Michigan, Ann Arbor, MI, USA, and the Director of the Automotive Research Center, Ann Arbor, a university-based U.S. Army Center of Excellence in Modeling and Simulation of Ground Vehicles. She has co-authored a book entitled *Control of Fuel Cell Power Systems*, 10 U.S. patents, and 200 publications on estimation and control of internal combustion engines and electrochemical processes, such as fuel cells and batteries.

Dr. Stefanopoulou is a fellow of the American Society of Mechanical Engineers (ASME), the Inaugural Chair of the ASME DSCD Energy Systems Technical Committee, a member of the SAE Dynamic System Modeling Standards Committee, and a member of the U.S. National Academies Committee on Vehicle Fuel Economy Standards. She has received five best paper awards.

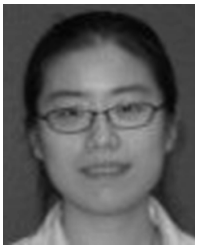

Li Jiang received the bachelor's degree in mechanical engineering from Shanghai Jiao Tong University, Shanghai, China, and the master's degree in electrical engineering and the Ph.D. degree in mechanical engineering from the University of Michigan, Ann Arbor, MI, USA.

She is currently the Manager of Advanced and System Engineering with Gasoline Systems North America, Robert Bosch LLC, Pittsburgh, PA, USA, where she is leading control system development for engine management system applications. She is also the Co-Principal Investigator of the Bosch and U.S. Department of Energy joint research projects on Advanced Combustion Concepts–Enabling Systems and Solutions.

Dr. Jiang was a recipient of the Recirculated Exhaust Gas Intake Sensing Award.